Supplementary Information for: "Breaking the ice: Identifying hydraulically-forced crevassing"

T.S. Hudson[1*], A.M. Brisbourne[2], R.S. White[3], JM. Kendall[1], R. Arthern[2], A.M. Smith[2]

[1] *Department of Earth Sciences, University of Oxford, Oxford, UK*

[2] *British Antarctic Survey, Cambridge, UK*

[3] *Bullard Laboratories, University of Cambridge, Cambridge, UK*

Corresponding author: Thomas S. Hudson (thomas.hudson@earth.ox.ac.uk)

Supplementary Text S1: P-to-Rayleigh amplitude ratios and icequake depth

The P-to-Rayleigh-wave amplitude ratios are calculated by taking the maximum amplitude within specified windows, as shown for the observed icequake example in Figure S1a. Figure S1c and Figure S1d show the P-to-Rayleigh-wave phase arrivals for one station ~450 m from the source. The particle motion of the inferred Rayleigh-wave is elliptical, providing us with confidence that it is indeed a surface wave arrival. P-wave and Rayleigh-wave windows are of fixed duration for all events, as in Figure S1. The uncertainty in the observed P-to-Rayleigh-wave amplitude ratios is defined as the standard deviation of the noise signal observed in a window 1s prior to the P-phase arrivals. Uncertainty in the epicentral distances given in Figure 1 are defined as the epicentral uncertainty output from NonLinLoc (Lomax & Virieux, 2000). The same method of obtaining P-to-Rayleigh-wave amplitudes is employed for the 2D finite difference modelled seismograms for various source depths from E3D (Larsen et al., 2001). The model is run for various source depths from 10 m to 120 m below surface, with the 2D interpolated field from the model runs (see Figure 2a) used to derive the likely crevasse depth from each receiver observation. These individual receiver observations are then combined for each icequake, to provide an overall estimate of the icequake depth. We independently verify crevasse depth by using S-P delay-times from receivers approximately directly above the crevasse. For the event in Figure S1, the S-P delay-time observed at a receiver approximately above the event is 0.014 s. With the velocity model shown in Figure 1b, this corresponds to an icequake depth of ~25 m below surface, compared to a depth of 29±12 m found using the P-to-Rayleigh amplitude ratios. We are therefore confident that the P-to-Rayleigh-wave amplitude ratios provide a good estimation of icequake depth.

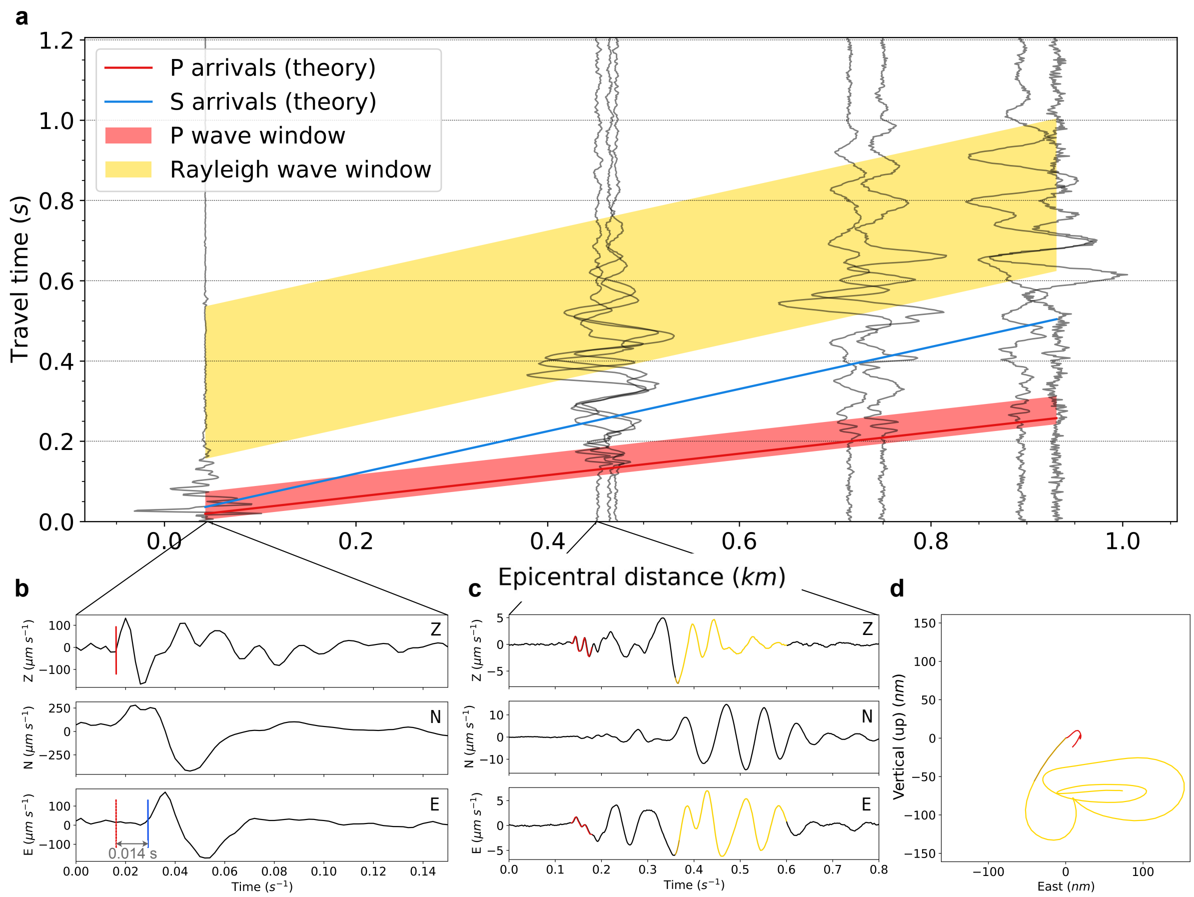

Supplementary Figure S1 – Example of observed waveforms at seismometers from a crevasse icequake at 14:33:52 on 28^th June 2014. a) Record section showing the P-to-Rayleigh-wave arrivals. The red and yellow regions show the windows used to calculate the P-to-Rayleigh amplitude ratios. b) Waveforms for an arrival 43 m from the event epicentre. P and S phase arrivals are indicated by the red and blue lines, respectively. c) Waveforms for an arrival 450 m from the event epicentre. d) Particle motions associated with the P and Rayleigh phase arrivals in (c). Red is the P-wave phase and yellow is the Rayleigh wave phase.

Supplementary Text S2: Derivation of maximum-dry-crevasse-depth

The maximum depth to which a crevasse can propagate without hydrofracture is governed by the tensile stress regime near the glacier surface. If the ice is under tensile stress then a crevasse can form. However, as the depth through the ice increases, the ice overburden pressure increases and acts to close the crevasse and prevent further fracture. At a certain depth, the maximum-dry-crevasse-depth, d^*, the maximum principal tensile stress acting to open crevasses becomes equal to the compressive ice overburden pressure. Below this depth, the ice overburden pressure is sufficiently high to prevent opening. This crevassing model is commonly referred to as the zero stress model (Colgan et al., 2016), and has been proven effective in predicting real crevasse depths (Mottram & Benn, 2009).

The above statement assumes that the ice will open under any net tensile stress, which is not strictly correct since the ice also has a tensile failure strength, that we do not account for here. Accounting for the tensile strength of the ice would simply make d^* shallower and hence increase the depth difference between icequake depths and the maximum-dry-crevasse-depth equipotential, therefore increasing the likelihood of icequakes observed being associated with hydrofracture. We also assume that there is a shallow firn layer at the glacier surface, of lower density than the underlying ice. This lower-density layer acts to make the maximum-dry-crevasse-depth deeper. We use the same local seismic refraction survey (Gudmundsson, 1989) as used to constrain the seismic velocities in Figure 1b to constrain the density profile of this layer, making the assumption that the change in velocity in the firn-layer is dominated by density rather than the bulk and shear moduli. This simplified firn density correction is assumed adequate for the purposes of this study since the weight estimation of the firn layer is conservative, therefore resulting in an overestimate of the maximum-dry-crevasse-depth.

To find d^*, one has to calculate the stress field near the glacier surface. This can be approximately obtained using the glacier surface velocity field. For a given point on the glacier, the velocity is defined by,

$$\overrightarrow{v_{i,j}} = \begin{pmatrix} u_{i,j} \\ v_{i,j} \\ w_{i,j} \end{pmatrix}, \qquad (3)$$

where u, v and w are the velocities in the x, y and z directions, and i, j denotes a particular horizontal location within the velocity field. To obtain the velocity field for the glacier surface at Skeidararjökull, we use GPS location data from the seismometers shown in Figure 2. The GPS data from the seismometers is more poorly constrained compared to dedicated dual-frequency GPS instruments, and is sampled only once per hour. Therefore, in order to reduce the GPS noise, we use a seven day moving average for the latitude, longitude and elevation data. We then calculate the average velocity over the ten day period of analysis. Even after applying this processing, data from only 7 stations are of sufficient quality to use. We then perform a two-dimensional, second-order interpolation for these velocity data points in order to obtain a horizontal velocity field for the network area. Due to only one station, SKR12, constraining the velocity field for the upper half of the network area, the interpolation scheme performs poorly outside the network, so we only analyse the velocity field approximately within the network, as shown in Figure 2 and Figure S2.

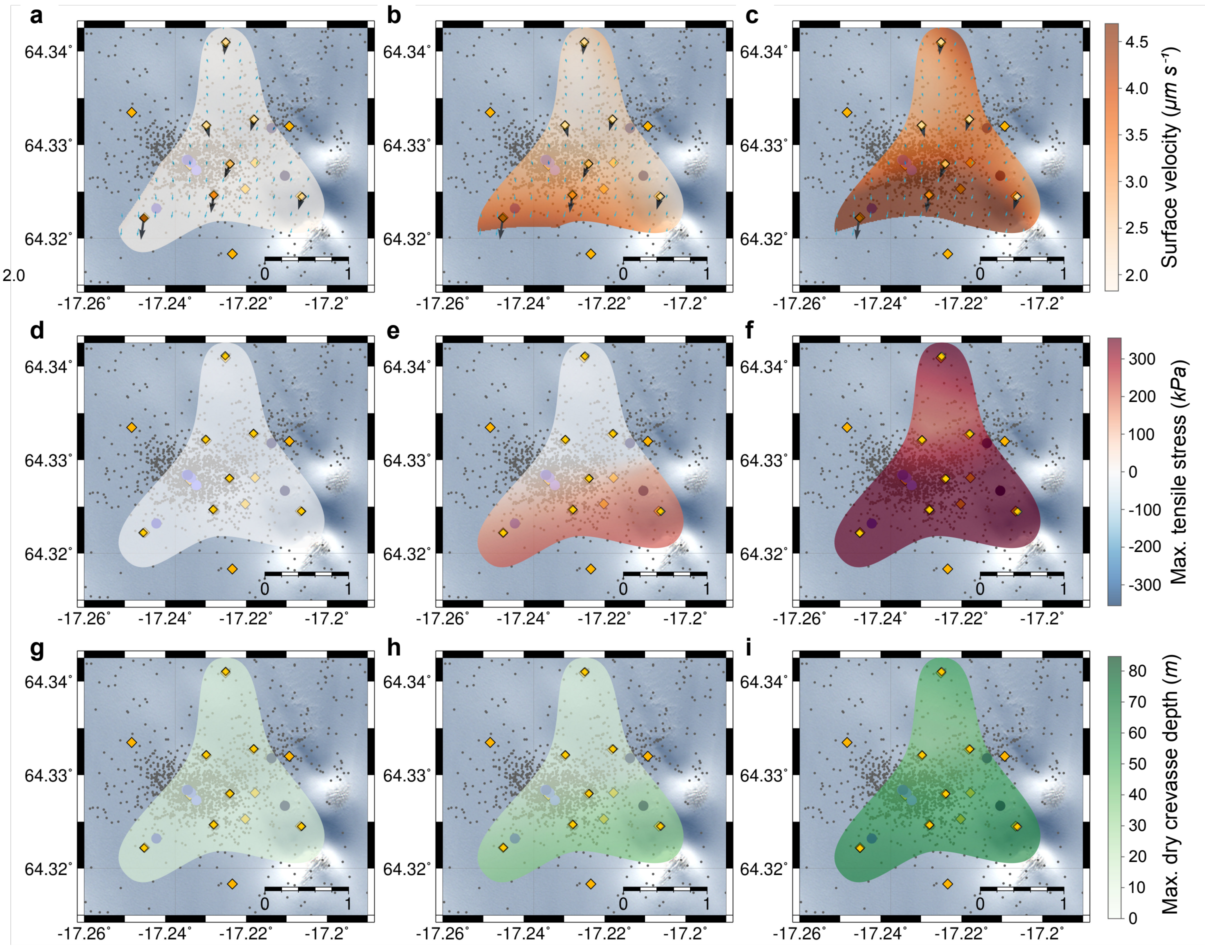

Figure S2 - The estimated uncertainty in the interpolated maximum surface velocity, maximum principal tensile stress and maximum-dry-crevasse-depth fields. (a) to (c) The lower, actual and upper uncertainty associated with the surface velocity field, respectively. (d) to (f) The lower, actual and upper uncertainty associated with the maximum principal stress field, respectively. (g) to (i) The lower, actual and upper uncertainty associated with the maximum-dry-crevasse-depth, respectively.

The velocity field can then be used to obtain the strain rate field for each point on the glacier surface. The second order strain rate tensor is given by,

$$\dot{\boldsymbol{\varepsilon}} = \begin{pmatrix} \dot{\varepsilon}_{xx} & \dot{\varepsilon}_{xy} & \dot{\varepsilon}_{xz} \\ \dot{\varepsilon}_{xy} & \dot{\varepsilon}_{yy} & \dot{\varepsilon}_{yz} \\ \dot{\varepsilon}_{xz} & \dot{\varepsilon}_{yz} & \dot{\varepsilon}_{zz} \end{pmatrix} = \begin{pmatrix} \frac{\partial u}{\partial x} & \frac{1}{2}\left(\frac{\partial u}{\partial y} + \frac{\partial v}{\partial x}\right) & 0 \\ \frac{1}{2}\left(\frac{\partial u}{\partial y} + \frac{\partial v}{\partial x}\right) & \frac{\partial v}{\partial y} & 0 \\ 0 & 0 & \frac{\partial w}{\partial z} \end{pmatrix}. \quad (4)$$

$\dot{\varepsilon}_{xz}$ and $\dot{\varepsilon}_{yz}$are taken to be zero, assuming no shear with depth, a realistic approximation near the glacier surface. If one also assumes that ice is incompressible, then $tr(\dot{\boldsymbol{\varepsilon}}) = 0$. $\dot{\varepsilon}_{zz}$ can then be found, giving,

$$\dot{\varepsilon}_{zz} = \frac{\partial w}{\partial z} = -\left(\frac{\partial u}{\partial x} + \frac{\partial v}{\partial y}\right). \quad (5)$$

To find the maximum-dry-crevasse-depth, we require the stress tensor. In order to calculate the stress tensor from the strain tensor, we need one final piece of information, the effective viscosity, η_{eff}, for a given horizontal location. Since ice behaves as a non-linear fluid, η_{eff} varies with the strain rate, $\dot{\boldsymbol{\varepsilon}}$. The effective viscosity is defined as,

$$\boldsymbol{\eta_{eff}} = \frac{B}{2}\left(\dot{\boldsymbol{\varepsilon}}_{\boldsymbol{eff}}\right)^{\frac{1}{n}-1}, \quad (6)$$

where B is given by,

$$B = A^{-\frac{1}{n}}, \quad (7)$$

where the temperature-dependent rate factor $A = 5.6 \times 10^{-17}\ Pa^{-3}\ a^{-1}$ and $n = 3$, determined from laboratory studies (Glen, 1955; Nick et al., 2010). The effective strain rate, $\dot{\boldsymbol{\varepsilon}}_{\boldsymbol{eff}}$, is defined by,

$$\dot{\boldsymbol{\varepsilon}}_{\boldsymbol{eff}} = |\dot{\boldsymbol{\varepsilon}}| = \left(\frac{1}{2}\ tr(\dot{\boldsymbol{\varepsilon}} \,.\, \dot{\boldsymbol{\varepsilon}})\right)^{\frac{1}{2}}. \quad (8)$$

The net stress tensor, $\boldsymbol{\sigma}$, is then defined as the difference between the opening stress and the ice overburden stress tensor by,

$$\boldsymbol{\sigma} = \boldsymbol{\sigma_{opening}} - \boldsymbol{\sigma_{overburden}}\,, \quad (9)$$

which can be written explicitly as,

$$\boldsymbol{\sigma} = \begin{pmatrix} 4\eta_{eff}\varepsilon_{xx,i,j} + 2\eta_{eff}\varepsilon_{yy} & 2\eta_{eff}\varepsilon_{xy} & 0 \\ 2\eta_{eff}\varepsilon_{xy} & 4\eta_{eff}\varepsilon_{yy} + 2\eta_{eff}\varepsilon_{xx} & 0 \\ 0 & 0 & 0 \end{pmatrix} - \rho g z \boldsymbol{I}\,, \quad (10)$$

where ρ is the ice density, g is the gravitational constant of acceleration and z is the depth below the ice surface. $\sigma_{opening,xz}$ and $\sigma_{opening,yz}$ are zero since we have assumed no vertical shear stress with depth and $\sigma_{opening,zz}$ is zero, assuming that the ice is in hydrostatic equilibrium. At the maximum-dry-crevasse-depth is where the maximum principal opening stress equals the overburden stress, at which point z is the maximum-dry-crevasse-depth, d^*. Therefore, to find d^* we need to find the maximum principal opening stress, $\boldsymbol{\sigma^*_{opening}}$. To do this, we rotate $\boldsymbol{\sigma}$ to maximise the tensile stress,

$$\boldsymbol{\sigma^*_{opening}} = \boldsymbol{S}\,\boldsymbol{\sigma_{opening}}\,\boldsymbol{S^T}, \quad (11)$$

where **S** is a rotation matrix comprising the eigenvectors of $\boldsymbol{\sigma_{opening}}$. The maximum-dry-crevasse-depth at a given point on the glacier surface, d^*, is then given by (Nick et al., 2010),

$$d^* = \frac{max\left(\boldsymbol{\sigma^*_{opening}}\right)}{\rho g}. \quad (12)$$

The uncertainty associated with the maximum-dry-crevasse-depth field is proportional to the uncertainty in the velocity field. To estimate the uncertainty, we calculate the standard deviation in the average velocity data and randomly perturb the velocity data used to calculate the velocity field by gaussian distributions about the average observed velocities, with the standard deviations used to constrain the width of these distributions. These gaussian distributions are sampled 1000 times. We then calculate the strain, stress, and crevasse depth fields from each perturbed velocity field, and define the lower and upper uncertainties for each field as the minimum and maximum values, respectively, for each point spatially within the fields. This data is shown by the red dashed lines in Figure 2d, and all the fields and their associated uncertainties are shown in Figure S2.

Supplementary references (also cited in main text)

Colgan, W., Rajaram, H., Abdalati, W., Mccutchan, C., Mottram, R., Moussavi, M. S., & Grigsby, S. (2016). Glacier crevasses: Observations, models, and mass balance implications. *Reviews of Geophysics*, *54*, 119–161. https://doi.org/10.1002/2015RG000504

Glen, J. W. (1955). The creep of polycrystalline ice. *Proceedings of the Royal Society of London. Series A, Mathematical and Physical Sciences*, *228*(1175), 519–538. https://doi.org/10.1098/rspa.1955.0066

Gudmundsson, M. T. (1989). The Grimsvotn Caldera, Vatnajokull: Subglacial Topography and Structure of Caldera Infill. *Jokull*, *39*, 3–7.

Mottram, R. H., & Benn, D. I. (2009). Testing crevasse-depth models: a field study at Breiðamerkurjokull, Iceland. *Journal of Glaciology*, *55*(192), 746–752.

Nick, F. M., Van Der Veen, C. J., Vieli, A., & Benn, D. I. (2010). A physically based calving model applied to marine outlet glaciers and implications for the glacier dynamics. *Journal of Glaciology*, *56*(199), 781–794.